Emergent kinetic constraints, ergodicity breaking, and cooperative dynamics in noisy quantum systems

B. Everest, M. Marcuzzi, J. P. Garrahan, and I. Lesanovsky

School of Physics and Astronomy, University of Nottingham, Nottingham NG7 2RD, United Kingdom
and Centre for the Mathematics and Theoretical Physics of Quantum Non-equilibrium Systems, University of Nottingham,
Nottingham NG7 2RD, United Kingdom

Kinetically constrained spin systems play an important role in understanding key properties of the dynamics of slowly relaxing materials, such as glasses. Recent experimental studies have revealed that manifest kinetic constraints govern the evolution of strongly interacting gases of highly excited atoms in a noisy environment. Motivated by this development we explore which types of kinetically constrained dynamics can generally emerge in quantum spin systems subject to strong noise and show how, in this framework, constraints are accompanied by conservation laws. We discuss an experimentally realizable case of a lattice gas, where the interplay between those and the geometry of the lattice leads to collective behavior and time-scale separation even at infinite temperature. This is in contrast to models of glass-forming substances which typically rely on low temperatures and the consequent suppression of thermal activation.

I. INTRODUCTION

Understanding and characterizing the dynamics of strongly interacting many-body systems remains a relevant challenge. This is even more the case in the context of systems undergoing complex collective relaxation such as glass formers which, under certain conditions (typically, below a certain temperature), display extremely long relaxation times [1–7]. One approach proposed to explain this dynamical behavior assumes that on the microscopic level local transitions are only permitted when certain conditions, e.g., very specific arrangements of particles, are satisfied. These so-called kinetic constraints [4,8–11] can produce dramatic effects on the dynamics: at sufficiently high densities or low temperatures there are severe restrictions on the allowed pathways that connect different many-body configurations.

Depending on the specific mechanism, kinetically constrained models (KCMs) can be grouped into classes [4], such as constrained (dynamic) lattice gases [12,13], where a particle's diffusion is hindered by its neighbors, mimicking excluded volume in dense fluids. Another instance is given by facilitated spin models, such as the so-called East [14] and Fredrickson-Andersen (FA) models [15], in which a spin's ability to update its state depends on the configuration of the ones nearby. Most KCMs consist of stochastic processes which end up in trivial steady states ρ_{ss} (e.g., for the East and FA models, $\rho_{ss} \propto e^{-\beta N}$ with N the number of excited (up) spins and β the inverse temperature) but feature dynamical rules which make the approach to stationarity highly intricate, often resulting in the emergence of metastability [4,9,10,14,15].

Despite their success in capturing many aspects of slow collective relaxation, it is hard to derive kinetic constraints from first principles as they seem to be an effective feature that only emerges in dense fluids after coarse-graining away fast short-scale motion [16]. However, it was recently shown that they naturally emerge in quantum optical systems [17–19], specifically cold atomic gases, in the presence of strong interactions and dephasing noise. In certain regimes, these systems show aspects of the facilitation dynamics [20,21] inherent to the FA and East models, as highlighted in recent experiments

[22,23]. KCMs have also been studied in the context of quantum annealing [24,25]. Kinetic constraints, moreover, govern the nonequilibrium dynamics of nuclear ensembles undergoing so-called dynamic nuclear polarization [26]—a process used to enhance the signal in magnetic resonance imaging applications—and have been found relevant in studies related to many-body localization [27,28].

Here we explore kinetic constraints that emerge in noisy quantum systems from a general perspective. Typically, KCMs rely on suppressed thermal activation to induce cooperative dynamics. This suppression mechanism is absent in noisy atomic systems which are coupled to a bath of effectively infinite temperature. We show that, nevertheless, strongly cooperative and glasslike behaviors may emerge in this framework. First we establish a connection between quantum optical systems and KCMs on a general basis, the underlying mechanism of which hinges upon the presence of (approximate) conservation laws. The resulting fragmentation of the space of states can make even the evolution towards an infinite temperature state highly complex. To demonstrate this, we then discuss an example of an effective reaction-diffusion process in which the interplay between these conservation laws and the lattice geometry induces cooperative diffusion. This experimentally realizable case displays pronounced collective behavior, time-scale separation, as well as ergodicity breaking due to the dynamical reducibility of the state space—features that are typically present in glassy dynamics.

II. CONSTRUCTION OF KINETICALLY CONSTRAINED SPIN SYSTEMS

We focus here on spin-$\frac{1}{2}$ systems (with internal states $|\uparrow\rangle$, $|\downarrow\rangle$) arranged on a regular lattice—whose L sites are labeled by k—with the standard spin operators

$$\sigma_k^+ = |\uparrow_k\rangle\langle\downarrow_k|, \tag{1}$$

$$\sigma_k^- = (\sigma_k^+)^\dagger, \tag{2}$$
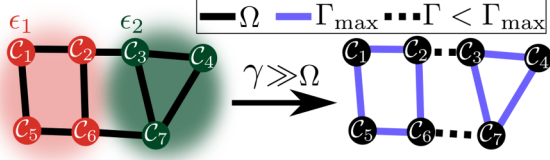
$$\sigma_k^z = [\sigma_k^+, \sigma_k^-]. \tag{3}$$

FIG. 1. Connectivity of the configuration space. Without noise (left), i.e., dephasing rate $\gamma = 0$, classical configurations, $|\mathcal{C}_m\rangle$, shown as circles, are connected to each other by H_Q with coupling strength $\propto \Omega$. In this example H_C is constructed such that the energy landscape in configuration space is separated into two plateaus with energies ϵ_1 (red) and ϵ_2 (green). This choice leads, in the presence of strong noise (right-hand side), to two weakly connected spaces. The transition rates within and between the domains are Γ and $\Gamma_{\max}$, respectively. For $\Gamma_{\max} \gg \Gamma$ this results in an (approximate) ergodicity breaking. For further explanation see text.

The coherent evolution is governed by a Hamiltonian $H = H_C + H_Q$ which we separate into a "classical" and a "quantum" part. The former assumes the form

$$H_C = \sum_k u_k n_k + \sum_{k,j} \frac{v_{kj}}{2} n_k n_j + \sum_{k,j,i} \frac{w_{kjl}}{3!} n_k n_j n_l + \cdots ,$$
(4)

where $n_k = (\sigma_k^z + 1)/2 = |\uparrow_k\rangle\langle\uparrow_k|$ and u_k, v_{kj}, and w_{kjl} can be interpreted as one-, two-, and three-body interaction couplings. In general, it can be any function of the number operators n_k. H_C defines an energetic landscape E_m over the classical (Fock) configurations $|\mathcal{C}_m\rangle = |\cdots \uparrow_{k-1} \uparrow_k \downarrow_{k+1} \cdots\rangle$ $(m = 1, \ldots, 2^L)$ via $H_C|\mathcal{C}_m\rangle = E_m|\mathcal{C}_m\rangle$. In Fig. 1, these configurations are represented as circles and grouped in domains of equal energy.

The quantum part acts as $H_Q|\mathcal{C}_m\rangle = \sum_{n \neq m} a_{mn}|\mathcal{C}_n\rangle$ and defines the "dynamical connectivity" of the configurations. This is illustrated in Fig. 1 where the solid lines correspond to the cases in which $a_{mn} \neq 0$. Here we focus on two prototypical examples: spin flipping, induced, e.g., by a laser on a two-level atomic transition which is commonly implemented in Rydberg atomic systems [29–31], and quantum tunneling of hard-core bosons between nearest neighbors [32,33], which are described by the Hamiltonians

$$H_Q^{(f)} = \Omega \sum_k \sigma_k^x \quad \text{and} \quad H_Q^{(t)} = \Omega \sum_{\langle k,j \rangle} \sigma_k^- \sigma_j^+, \quad (5)$$

respectively. Here $\langle k, j \rangle$ is shorthand for summing over nearest neighbors only, $\sigma_k^x = \sigma_k^+ + \sigma_k^-$, and Ω is the coupling strength of the two processes (i.e., depending on the realization: the laser Rabi frequency, the exchange coupling, or lattice tunneling amplitude).

The system is in contact with an environment which induces fast decoherence of quantum superpositions. We assume the noise to be white and spatially uncorrelated, so that the evolution of the density matrix ρ is governed by the Lindblad equation [34,35]

$$\dot{\rho} = -i[H,\rho] + \gamma \sum_{k}^{L} \left(n_k \rho n_k - \frac{1}{2}\{n_k,\rho\} \right), \quad (6)$$

where $\{A, B\} = AB + BA$ denotes anticommutation and γ is the dephasing rate. This form of dissipation occurs naturally in cold atom lattice experiments, stemming, e.g., from the off-resonant scattering of photons from the optical-trapping laser field [36], or from phase noise of the laser driving [22,23,37]. We further set $\gamma \gg \Omega$, relying on the possibility of independently tuning these two parameters [32,36] (see also the Supplemental Material [38]). This allows the adiabatic elimination of H_Q and the projection of the dynamics onto the subspace of diagonal density matrices μ in the $|\mathcal{C}_m\rangle$ basis [17,39–43]. The reduced state μ can then be interpreted as a probability distribution and evolves according to the classical master equation

$$\partial_t \mu = \sum_\nu \frac{4}{s\gamma} \Gamma_\nu (l_\nu^\dagger \mu l_\nu + l_\nu \mu l_\nu^\dagger - \{l_\nu, l_\nu^\dagger\}\mu), \quad (7)$$

where the operators l_ν, the index ν, and the coefficient s depend on the choice of H_Q. In the case of spin flipping, $H_Q^{(f)}$, the sum runs over the sites $\nu \equiv k$, $s = 1$, and $l_k = \Omega\sigma_k^+$. For tunneling, instead, the sum runs over neighboring pairs $\nu \equiv \langle kj \rangle$, $s = 2$, and $l_{kj} = \Omega\sigma_k^+ \sigma_j^- / \sqrt{2}$. The rates Γ_ν are configuration dependent and read

$$\frac{1}{\Gamma_\nu} = 1 + \left(\frac{2\,\delta E}{s\gamma} \right)^2, \quad (8)$$

where δE is the "energy cost" of performing the l_ν-induced transition (see Ref. [38]). More precisely, when $l_\nu|\mathcal{C}_m\rangle \propto |\mathcal{C}_n\rangle$ then $\delta E = E_n - E_m$. Note that the inverse process induced by $l_\nu^\dagger$ occurs at the same rate; therefore, Eq. (7) satisfies detailed balance at infinite temperature and the steady-state distribution μ_{ss} is uniform ($\propto \mathbb{1}$ under ergodic conditions).

III. "HARD" AND "SOFT" KINETICALLY CONSTRAINED MODELS

According to Eq. (8) the rate of a transition is maximal when both involved states are on resonance, i.e., $\delta E = 0$. Conversely, if $|\delta E| \gg \gamma$ the transition rate is greatly suppressed. This implies that, depending on the precise form of H_C, particular processes can be favored over others, constraining in turn the dynamics to favor specific pathways in configuration space.

In the limit $|\delta E|/\gamma \to \infty$ the suppression is total and the corresponding transition is "blocked." Ideally, in a context where energy differences are either vanishing or infinite, one obtains a *hard* constraint, and transitions induced by H_Q either take place at rate $\Gamma_{\max} = 1$ or never occur ($\Gamma = 0$). As highlighted in Fig. 1, this causes the space to fragment into disconnected parts (corresponding to different energies), breaking ergodicity and producing a reducible dynamics. Necessarily, any kinetic constraint prohibiting a transition between two configurations ($|\mathcal{C}_1\rangle \not\to |\mathcal{C}_2\rangle$) can only admit a hard realization if there is no sequence of allowed transitions connecting them.

If such a pathway exists, (e.g., $|\mathcal{C}_1\rangle \to |\mathcal{C}_3\rangle \to |\mathcal{C}_2\rangle$), the realization of a *soft* constraint [44] might still be possible. In this case direct transitions between $|\mathcal{C}_1\rangle$ and $|\mathcal{C}_2\rangle$ cannot be forbidden but merely suppressed. The degree of suppression is determined by the minimal number q of allowed transitions joining $|\mathcal{C}_1\rangle$ and $|\mathcal{C}_2\rangle$ and is $\Gamma_{\mathrm{suppressed}}/\Gamma_{\mathrm{allowed}} \gtrsim 1/q^2$.

It may be of interest at this point to remark on the differences between the mechanism highlighted here and the one underlying quantum annealing of KCMs in previous studies [24,25]. First, the long-time dynamics considered in our work is not an annealed one, as the system heats up under the action of the dephasing noise. This is in contrast to an annealing procedure which seeks to decrease temperature. Second, instead of relying on quantum tunneling through potential barriers (between quasiresonant local states), our approach to restrict the system's dynamics to a specific manifold of states relies on the suppression of transitions to much higher or much lower energies, which effectively reproduces constraints as sketched in Fig. 1.

IV. REACTION-DIFFUSION MODEL WITH CONSTANT BONDS

Based on the above discussion, we construct here a KCM which mimics a lattice gas with excluded volume effects. This model admits a hard realization and is simple enough to be experimentally realizable with cold atoms in an optical lattice (see Refs. [36,45]). It consists of particles arranged on a triangular lattice which feature nearest-neighbor tunneling, as given by $H_Q^{(t)}$ in Eq. (5), and strong nearest-neighbor interactions, $H_C = U \sum_{\langle k,j \rangle} n_k n_j$. In the presence of dephasing this leads to a stochastic process of excitations (up spins) hopping with rates that depend on the interaction strength U. The number of excitations N is conserved by construction. Taking the limit $U/\gamma \to \infty$ introduces a further conserved quantity, namely the number B of neighboring pairs of excitations (bonds). Consequently, excitations can only hop if doing so preserves the number of bonds between them.

Clusters of excitations become bound structures, whose dynamical behavior strongly depends on their shape. Two primary examples are shown in Fig. 2. The first is a "polymer," consisting of two or more excitations arranged along a chain, which can only diffuse via slow, cooperative motion [46]. The
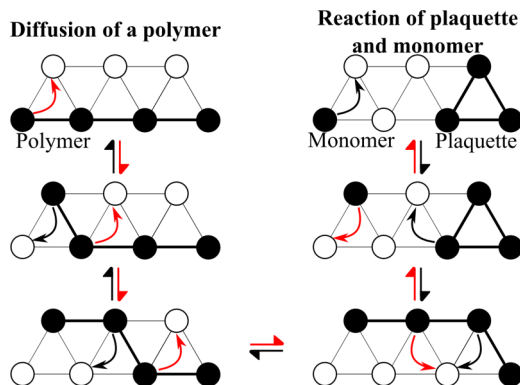

FIG. 2. Illustrations of key processes governing the dynamics of the reaction-diffusion model with constant bonds. The black dots represent excitations and a thick line on the lattice represents a bond. Arrows denote possible moves and point at the resulting configurations. A polymer (left) is a chain of connected excitations, and shown is the way in which it can diffuse across the lattice. A plaquette (right) is formed by three excitations filling the vertices of a triangular tile. We showcase its reaction with a monomer.
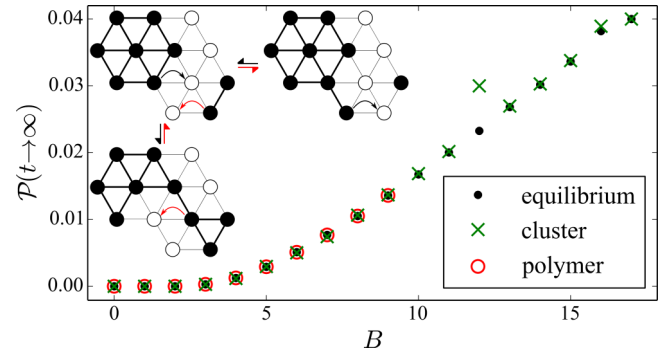

FIG. 3. Stationary plaquette density $\mathcal{P}(t \to \infty)$ against the number of bonds B for a 10×10 lattice with $N = 10$, obtained via two different averaging procedures: Black dots are calculated from a uniform random sampling of configurations at fixed (N,B). The remaining data points are averages over different realizations of the dynamics via a kinetic Monte Carlo procedure, differing by the initial condition: green crosses indicate a single cluster plus monomers, where the former is chosen to be as compact as possible; red circles indicate a single polymer plus monomers. The inset shows how the cluster present at $B = 13$ can react with a monomer and the one at $B = 12$ with a dimer. The numerical error here is smaller than the size of the markers and thus not displayed.

second is a "plaquette," three excitations at the vertices of the same triangular tile. The plaquette is the simplest example of an immobile structure which cannot diffuse by itself, since any hop would result in the net loss of (at least) a bond. It can, however, react with "monomers" (isolated excitations) or other mobile structures (see right-hand side of Fig. 2). This leads to an assisted diffusion which is reminiscent of the strongly cooperative motion found in many glassy models [4,9,10,14,15].

Interestingly, N and B do not exhaust all the conservation laws of this model. There are additional, subtler ones that further split the space of configurations. Consider, for example, the case $N = B = 3$, which encompasses all possibilities of placing a single plaquette in the lattice: since plaquettes are unable to move on their own, all these states are dynamically disconnected. This finer structure is generally related to the formation of immobile clusters and thus emerges at high numbers of bonds, $B \gtrsim N$. This is exemplified in Fig. 3, where we compare results obtained from dynamical simulations with estimates based upon assuming that the steady state is an equilibrium "microcanonical shell" at fixed (N,B). Without this additional dynamical reduction, the two predictions would coincide. Shown is the plaquette density $\mathcal{P} = $ (number of plaquettes/$2L$) in a 10×10 lattice with $N = 10$ excitations and different values of B from 0 to 17. The black dots are averages obtained from uniform random samplings of states at fixed (N,B). The other data sets correspond to long-time values of $\mathcal{P}$ extracted from kinetic Monte Carlo simulations of the dynamics. The initial conditions are chosen either to have all bonds taken by a single polymer structure (red circles), which is only possible up to $B = N - 1 = 9$, or to have all bonds taken by the smallest possible cluster (green crosses). In both cases, the remaining excitations are introduced as monomers.
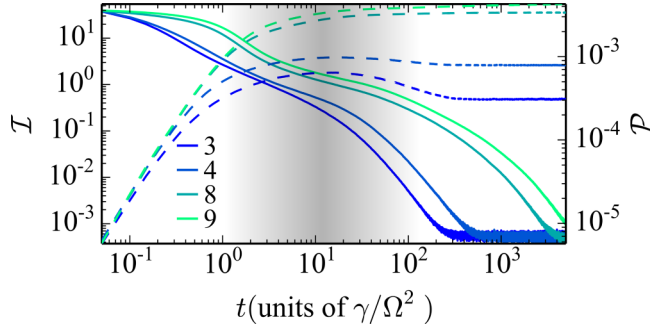
FIG. 4. Dynamics of the imbalance $\mathcal{I}$ (solid) and plaquette density $\mathcal{P}$ (dashed) for a 20×20 lattice with $N = 10$. All cases are initialized with a single $(B + 1)$ polymer and $N - B - 1$ monomers for $B = 3, 4, 8,$ and 9. The relaxation time increases with B. At low B, the plaquette density overshoots its stationary value and correspondingly the decay of the imbalance speeds up. This highlights the advantage in liberating monomers (or smaller structure) by forming plaquettes. The subsequent assisted diffusion of plaquettes acts on much longer time scales and eventually reduces $\mathcal{P}$ to its stationary value. The shaded area marks the separation between two regimes in the dynamics, the earliest dominated by plaquette creation and monomer diffusion, the latest by assisted diffusion of plaquettes. The errors on $\mathcal{I}$ and $\mathcal{P}$ are of order 10^{-5} and 10^{-6}, respectively.

At a sufficiently low number of bonds, B, there are no appreciable deviations and most configurations with the same (N, B) are dynamically connected. For $B = 12$ and 16, however, the "cluster initialization" displays a higher stationary plaquette density than the naive equilibrium value. For instance, the initial cluster at $B = 12$ is chosen to be the "filled hexagon" displayed in the top-left corner of Fig. 3. Monomers cannot react with it, since each of the outer excitations forms three bonds. In order to break it apart, the assistance of a dimer (or longer polymer) is required. Therefore, this structure is inert, while the remaining monomers explore the rest of the lattice via ordinary diffusion. Note, however, that adding bonds does not necessarily make a structure less prone to dissolution: for $B = 13$ the initial cluster can react with monomers via the mechanism displayed in Fig. 3, starting from the top-right configuration.

The presence of complex structures which cannot move by themselves and can only undergo assisted diffusion results in a separation of time scales in the dynamics, as displayed in Fig. 4. There we report the evolution of the *imbalance*

$$\mathcal{I} = \sum_{\langle k, j \rangle} |\langle n_k \rangle - \langle n_j \rangle|^2, \tag{9}$$

a measure of the nonuniformity of the system, and the plaquette density $\mathcal{P}(t)$ as a function of time for a 20×20 lattice, $N = 10$, and prepared at $t = 0$ in a single-polymer state with $B = 3, 4, 8,$ and 9. These configurations can explore the entire lattice and thus restore translational invariance for sufficiently long times, implying $\mathcal{I}(t \to \infty) \to 0$. The early dynamics is dominated by diffusion of the original structures (predominantly monomers) and formation of plaquettes. For the low-B cases, around $t \approx 10\gamma/\Omega^2$ the plaquette density reaches its maximum, which is higher than its stationary value. Correspondingly, the imbalance relaxation speeds up, which can be understood as follows: the formation of clusters such

as plaquettes breaks down polymers to shorter ones, which display higher mobility and diffuse faster. For instance, for $B = 3$, once a plaquette is formed an additional monomer is released (see Fig. 2) and monomers are the most efficient objects at exploring the lattice. Consequently, the higher the plaquette density, the higher the rate of relaxation of the imbalance. On longer time scales, further plaquette-monomer reactions relax $\mathcal{P}$ to its actual stationary value.

V. FACILITATED SPIN MODELS

For completeness, we comment here on the realizability of the aforementioned (one-dimensional) FA and East models [4]. Both feature facilitated spin flipping [$H_Q^{(f)}$ in Eq. (5)], whereby an excitation (up spin) enables the flipping of its neighbors, e.g., $\uparrow\uparrow\downarrow \rightleftarrows \uparrow\uparrow\downarrow$ (whereas $\downarrow\uparrow\downarrow \not\rightleftarrows \downarrow\downarrow\downarrow$). In the East model, facilitation is further constrained and can only take place to an excitation's right. Neither model admits a hard realization. To see this we consider the transition $\uparrow\downarrow\downarrow\downarrow \to \uparrow\downarrow\uparrow\downarrow$ which must be forbidden in both models. However, both configurations can be connected via a sequence of allowed steps $\uparrow\downarrow\downarrow\downarrow \to \uparrow\uparrow\downarrow\downarrow \to \uparrow\uparrow\uparrow\downarrow \to \uparrow\downarrow\uparrow\downarrow$. The FA model still admits a soft realization [choosing $H_C = U \sum_k n_k(1 - 2n_{k+1}/3)$] with $\Gamma_{\text{suppressed}}/\Gamma_{\text{allowed}} \gtrsim 1/9$.

Furthermore, for the facilitated dynamics inherent to the FA and East models to display glassy features, it is crucial that the density of excitations (up spins) remains low. Conversely, under Eq. (7) the state invariably evolves towards equilibrium at infinite temperature, which poses a severe restriction to its applicability in this case. However, introducing additional noise sources might provide a way around, as it may change the nature of the stationary state (see Refs. [17,21,37,47,48]).

VI. CONCLUSIONS

Kinetically constrained models were originally introduced to capture the basic properties of slow-relaxing materials, yet have largely remained an idealized construct. Here we have shown that in the presence of strong noise these constraints emerge rather naturally in the dynamics of experimentally realizable open quantum systems.

An interesting question is whether, and how, the collective behavior discussed here changes when quantum coherence is not entirely washed out by the noise. This could be systematically addressed in an experimental realization of the discussed reaction-diffusion model with cold atoms in lattices [49–51], thereby providing a handle for exploring quantum effects in glassy relaxation [52,53]. This could also shed light on the interplay between quantum and classical fluctuations on collective phenomena, as e.g. recently discussed in Refs. [54,55].

[1] L. C. Struik, *Physical Aging in Amorphous Polymers and Other Materials* (Elsevier, Amsterdam, 1978).

[2] S. Ciliberto, in *Slow Relaxations and Nonequilibrium Dynamics in Condensed Matter* (Springer, Berlin, 2003), Vol. 77, p. 555.

[3] K. Binder and W. Kob, *Glassy Materials and Disordered Solids: An Introduction to Their Statistical Mechanics* (World Scientific, Singapore, 2005).

[4] P. S. F. Ritort, Adv. Phys. **52**, 219 (2003).

[5] L. Peliti, *Statistical Mechanics in a Nutshell* (Princeton University Press, Princeton, NJ, 2011).

[6] G. Biroli and J. P. Garrahan, J. Chem. Phys. **138**, 12A301 (2013).

[7] L. Berthier and M. D. Ediger, Phys. Today **69**, 40 (2016).

[8] J. P. Garrahan and D. Chandler, Phys. Rev. Lett. **89**, 035704 (2002).

[9] J. P. Garrahan, R. L. Jack, V. Lecomte, E. Pitard, K. van Duijvendijk, and F. van Wijland, Phys. Rev. Lett. **98**, 195702 (2007).

[10] J. P. Garrahan, R. L. Jack, V. Lecomte, E. Pitard, K. van Duijvendijk, and F. van Wijland, J. Phys. A: Math. Theor. **42**, 075007 (2009).

[11] L. Berthier and G. Biroli, Rev. Mod. Phys. **83**, 587 (2011).

[12] W. Kob and H. C. Andersen, Phys. Rev. E **48**, 4364 (1993).

[13] V. Teboul, J. Chem. Phys. **141**, 194501 (2014).

[14] J. Jäckle and S. Eisinger, Z. Phys. B **84**, 115 (1991).

[15] G. H. Fredrickson and H. C. Andersen, Phys. Rev. Lett. **53**, 1244 (1984).

[16] A. S. Keys, L. O. Hedges, J. P. Garrahan, S. C. Glotzer, and D. Chandler, Phys. Rev. X **1**, 021013 (2011).

[17] I. Lesanovsky and J. P. Garrahan, Phys. Rev. Lett. **111**, 215305 (2013).

[18] D. Poletti, P. Barmettler, A. Georges, and C. Kollath, Phys. Rev. Lett. **111**, 195301 (2013).

[19] M. Mattioli, A. W. Glätzle, and W. Lechner, New J. Phys. **17**, 113039 (2015).

[20] M. Marcuzzi, E. Levi, W. Li, J. P. Garrahan, B. Olmos, and I. Lesanovsky, New J. Phys. **17**, 072003 (2015).

[21] B. Everest, M. Marcuzzi, and I. Lesanovsky, Phys. Rev. A **93**, 023409 (2016).

[22] M. M. Valado, C. Simonelli, M. D. Hoogerland, I. Lesanovsky, J. P. Garrahan, E. Arimondo, D. Ciampini, and O. Morsch, Phys. Rev. A **93**, 040701(R) (2016).

[23] A. Urvoy, F. Ripka, I. Lesanovsky, D. Booth, J. P. Shaffer, T. Pfau, and R. Löw, Phys. Rev. Lett. **114**, 203002 (2015).

[24] A. Das, B. K. Chakrabarti, and R. B. Stinchcombe, Phys. Rev. E **72**, 026701 (2005).

[25] A. Das and B. K. Chakrabarti, Rev. Mod. Phys. **80**, 1061 (2008).

[26] A. Karabanov, D. Wiśniewski, I. Lesanovsky, and W. Köckenberger, Phys. Rev. Lett. **115**, 020404 (2015).

[27] J. M. Hickey, S. Genway, and J. P. Garrahan, J. Stat. Mech. Theory Exp. (2016) 054047.

[28] M. van Horssen, E. Levi, and J. P. Garrahan, Phys. Rev. B **92**, 100305 (2015).

[29] M. Saffman, T. G. Walker, and K. Mølmer, Rev. Mod. Phys. **82**, 2313 (2010).

[30] R. Löw, H. Weimer, J. Nipper, J. B. Balewski, B. Butscher, H. P. Büchler, and T. Pfau, J. Phys. B **45**, 113001 (2012).

[31] H. Labuhn, D. Barredo, S. Ravets, S. de Léséleuc, T. Macrì, T. Lahaye, and A. Browaeys, Nature (London) **534**, 667 (2016).

[32] I. Bloch, J. Dalibard, and W. Zwerger, Rev. Mod. Phys. **80**, 885 (2008).

[33] J. J. García-Ripoll, S. Dürr, N. Syassen, D. M. Bauer, M. Lettner, G. Rempe, and J. I. Cirac, New J. Phys. **11**, 013053 (2009).

[34] G. Lindblad, Commun. Math. Phys. **48**, 119 (1976).

[35] H. P. Breuer and F. Petruccione, *The Theory of Open Quantum Systems* (Oxford University Press, New York, 2002), p. 625.

[36] S. Sarkar, S. Langer, J. Schachenmayer, and A. J. Daley, Phys. Rev. A **90**, 023618 (2014).

[37] H. Schempp, G. Günter, M. Robert-de-Saint-Vincent, C. S. Hofmann, D. Breyel, A. Komnik, D. W. Schönleber, M. Gärttner, J. Evers, S. Whitlock, and M. Weidemüller, Phys. Rev. Lett. **112**, 013002 (2014).

[38] See Supplemental Material at http://link.aps.org/supplemental/10.1103/PhysRevE.94.052108 for the expressions of the tunneling and dephasing rates and for a brief derivation of the master equation.

[39] Z. Cai and T. Barthel, Phys. Rev. Lett. **111**, 150403 (2013).

[40] M. Marcuzzi, J. Schick, B. Olmos, and I. Lesanovsky, J. Phys. A: Math. Theor. **47**, 482001 (2014).

[41] P. Degenfeld-Schonburg and M. J. Hartmann, Phys. Rev. B **89**, 245108 (2014).

[42] J.-S. Bernier, D. Poletti, and C. Kollath, Phys. Rev. B **90**, 205125 (2014).

[43] B. Sciolla, D. Poletti, and C. Kollath, Phys. Rev. Lett. **114**, 170401 (2015).

[44] Y. S. Elmatad, R. L. Jack, D. Chandler, and J. P. Garrahan, Proc. Natl. Acad. Sci. U.S.A. **107**, 12793 (2010).

[45] O. Dutta, M. Gajda, P. Hauke, M. Lewenstein, D.-S. Lühmann, B. A. Malomed, T. Sowiski, and J. Zakrzewski, Rep. Prog. Phys. **78**, 066001 (2015).

[46] R. A. L. Jones, *Soft Condensed Matter* (Oxford University Press, New York, 2011).

[47] M. Hoening, W. Abdussalam, M. Fleischhauer, and T. Pohl, Phys. Rev. A **90**, 021603 (2014).

[48] D. W. Schönleber, M. Gärttner, and J. Evers, Phys. Rev. A **89**, 033421 (2014).

[49] W. S. Bakr, J. I. Gillen, A. Peng, S. Fölling, and M. Greiner, Nature (London) **462**, 74 (2009).

[50] W. S. Bakr, A. Peng, M. E. Tai, R. Ma, J. Simon, J. I. Gillen, S. Fölling, L. Pollet, and M. Greiner, Science **329**, 547 (2010).

[51] J. F. Sherson, C. Weitenberg, M. Endres, M. Cheneau, I. Bloch, and S. Kuhr, Nat. Phys. **467**, 68 (2010).

[52] T. E. Markland, J. A. Morrone, B. J. Berne, K. Miyazaki, E. Rabani, and D. R. Reichman, Nat. Phys. **7**, 134 (2011).

[53] B. Olmos, I. Lesanovsky, and J. P. Garrahan, Phys. Rev. Lett. **109**, 020403 (2012).

[54] M. Marcuzzi, M. Buchhold, S. Diehl, and I. Lesanovsky, Phys. Rev. Lett. **116**, 245701 (2016).

[55] M. Schreiber, S. S. Hodgman, P. Bordia, H. P. Lüschen, M. H. Fischer, R. Vosk, E. Altman, U. Schneider, and I. Bloch, Science **349**, 842 (2015).